

RESEARCH LETTER

10.1002/2014GL059942

Key Points:

- Distant fault (200 km) reactivated during the M7.6 Nicoya earthquake
- Threshold of remote triggering for the Nicoya earthquake
- New mechanism that combines dynamic stress triggering and elastic deformation

Correspondence to:

M. Lupi,
matteo.lupi@erdw.ethz.ch

Citation:

Lupi, M., F. Fuchs, and J. F. Pacheco (2014), Fault reactivation due to the M7.6 Nicoya earthquake at the Turrialba-Irazú volcanic complex, Costa Rica: Effects of dynamic stress triggering, *Geophys. Res. Lett.*, *41*, 4142–4148, doi:10.1002/2014GL059942.

Received 19 MAR 2014

Accepted 27 MAY 2014

Accepted article online 29 MAY 2014

Published online 17 JUN 2014

Fault reactivation due to the M7.6 Nicoya earthquake at the Turrialba-Irazú volcanic complex, Costa Rica: Effects of dynamic stress triggering

M. Lupi¹, Florian Fuchs², and Javier F. Pacheco³

¹ Geological Institute, ETH Zurich, Zurich, Switzerland, ² Steinmann Institute, Bonn University, Bonn, Germany,

³ Observatorio Vulcanológico y Sismológico de Costa Rica, Heredia, Costa Rica

Abstract The M7.6 Nicoya earthquake struck at the interface between the Cocos plate and the Caribbean plate on 5 September 2012 inducing a ground acceleration of 0.5 m s^{-2} at the Irazú-Turrialba volcanic complex. We use data from six seismic stations deployed around and atop the Irazú-Turrialba volcanic complex to show the increase of local seismic activity after the M7.6 Nicoya earthquake. The response consists in more than 300 locatable earthquakes occurring in swarm sequences along a fault system that intersects the Irazú-Turrialba volcanic complex. In addition, we point out that major aftershocks are followed by increases of seismic activity in the same region. The weak static stress variation imposed by the main slip of the Nicoya earthquake at the Irazú-Turrialba volcanic complex suggests a dynamic triggering mechanism. We expand this concept suggesting that this behavior may be similar to the one observed in the Chilean and Japanese volcanic arcs during the M8.8 2010 Maule, Chile, and M9.0 2011 Tohoku, Japan, earthquakes. Finally, we highlight that the combined action of dynamic stress and short-lived coseismic relaxation may trigger seismic activity in geological systems in near-critical conditions.

1. Introduction

Static and dynamic stresses generated by large magnitude earthquakes act at different timescales and distances. Static stress variations operate over decades and relatively short distances (the stress decays according to $1/R^3$, where R is the distance from the epicenter) [Hill *et al.*, 2002] while dynamic stress affects the near field and far field during the propagation of the seismic waves. Effects of moderate to large magnitude earthquakes in the near field and far field are well documented [e.g., Hill *et al.*, 2002; Marzocchi *et al.*, 2002; Walter *et al.*, 2007; Eggert and Walter, 2009] and include hydrogeological responses [Wang, 2007; Wang and Manga, 2010], triggered seismic activity [Husen *et al.*, 2004; West *et al.*, 2005; Hill and Prejean, 2007], temperature variations at hydrothermal systems [Johnson *et al.*, 2000; Dziak *et al.*, 2003], variations of water levels in boreholes [Roeloffs, 1998; Matsumoto *et al.*, 2003; Weingarten and Ge, 2014], triggered volcanic activity [Linde and Sacks, 1998; Manga and Brodsky, 2006; Walter *et al.*, 2007; Delle Donne *et al.*, 2010], and triggered mud volcanism [Mazzini *et al.*, 2007; Manga and Bonini, 2012; Lupi *et al.*, 2013]. In addition, earthquakes may promote the coseismic precipitation of gold deposits and induce mineral phase precipitation in hydrothermal systems [Weatherley and Henley, 2013]. Volcanic and hydrothermal environments are particularly sensitive to external perturbations because of the (often) critical conditions encountered at depth [e.g., van der Elst *et al.*, 2013].

The oblique subduction of the Cocos plate beneath the Caribbean plate imposes strain partitioning in the upper plate leading to intense and shallow seismic activity along a NW striking fault system (and the associated NE trending antithetic faults) running through the volcanic arc [Corti *et al.*, 2005; Lewis *et al.*, 2008; Montero *et al.*, 2013]. The maximum slip of the M7.6 Nicoya earthquake (5 September 2012, 14:42 UTC) was approximately 2.5 m ($\sim 9.76^\circ\text{N}$, 85.56°W) [Yue *et al.*, 2013]. It induced a ground acceleration greater than 4.9 m s^{-2} close to the epicenter [Protti *et al.*, 2014] and an average ground acceleration of 0.5 m s^{-2} near the Irazú-Turrialba volcanic complex (ITVC) [Yue *et al.*, 2013]. The ITVC is cut by the southernmost segment of the East Río Sucio Fault (ERSF), a right-lateral strike-slip system that joins the Finca Liebres volcanic depression between the Irazú and Turrialba volcanoes (Figure 1bottom). At the surface, this area is not characterized by any strong hydrothermal activity. The only hot thermal spring is Quebrada Peña (60°C), near the Turrialba volcano, while around the Irazú volcano sparse hot springs emissions range from 30°C to 60°C .

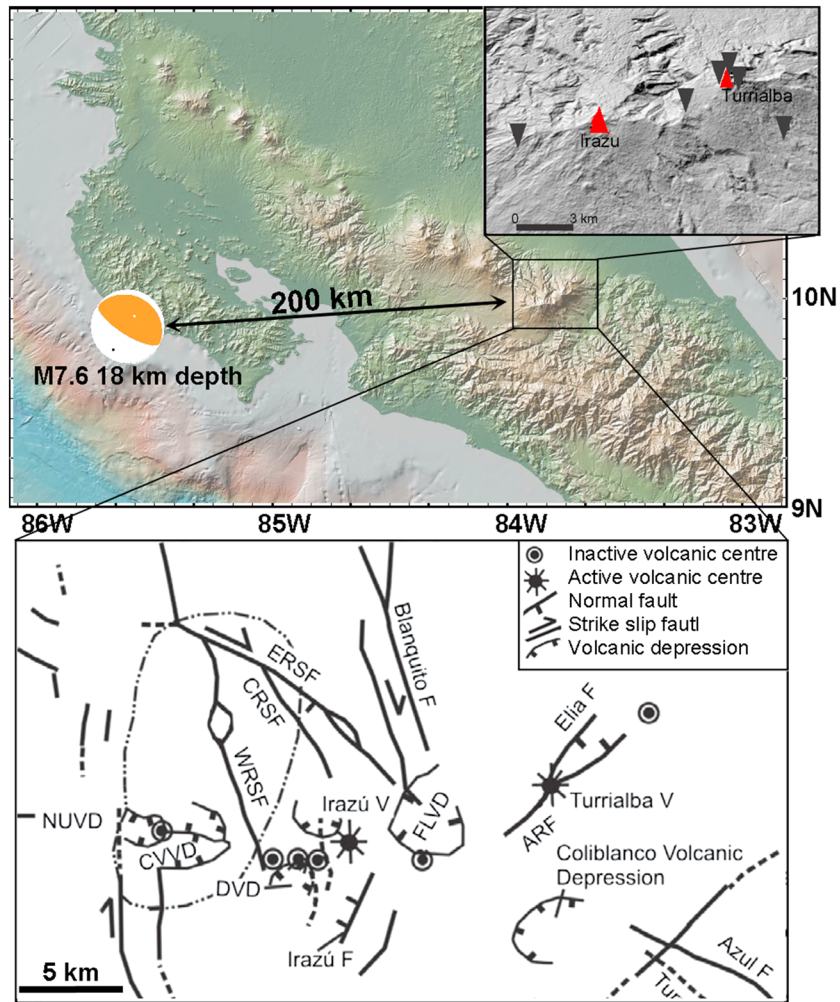


Figure 1. (top) Map of Costa Rica and tectonic setting around the Irazú and Turrialba volcanoes. The Nicoya earthquake occurred at the subduction interface, and the inverted fault plane solution shows almost a pure reverse slip. The gray-shaded inset shows the Irazú-Turrialba volcanic complex (red triangles show the main craters) and the distribution of the seismic stations (black triangles). The stations are deployed on volcanoclastic deposits due to the lack of suitable sites on bedrocks. However, the site amplification effect for the seismic stations around the ITVC affects the higher frequencies only (i.e., above 15 Hz). (bottom) The map (modified after *Montero et al.* [2013]) represents the tectonic features of this region including the East Río Sucio Fault (ERSF). Other abbreviations are for the Central Río Sucio Fault (CRSF), the West Río Sucio Fault (WRSF), and Finca Liebres Volcanic Depression (FLVD).

The last major eruption of the Irazú volcano occurred in 1963 (VEI = 3), while the most recent volcanic activity took place on the NW flank in 1994 and consisted of a small magnitude phreatic explosion [*Alvarado et al.*, 2006]. The Turrialba volcano was quiescent during the last century until the 5 January 2010 when a VEI = 2 eruption occurred at the SW crater. Activity at Turrialba continued with repeating explosions (VEI from 1 to 2) until May 2013 and returned to a dormant state in June 2013.

The Observatorio Vulcanológico y Sismológico de Costa Rica (OVSICORI) maintains a network of six seismic stations around the ITVC (Figures 1(top, inset) and 2) to monitor the volcanic activity of the area. After the M7.6 2012 Nicoya earthquake the network recorded more than 300 locatable seismic events occurring in swarm sequences during the 24 h following the main slip (Figure 2, top). In this occasion, the Irazú and Turrialba volcanoes behaved differently. Several events occurred around the Irazú volcano, while almost no seismic activity was recorded beneath the Turrialba volcano. We use data from the OVSICORI seismic network to shed light on the interaction between dynamic stresses and critically stressed geologic environments and to describe the occurrence of seismic activity along the ERSF after the M7.6 2012 Nicoya, Costa Rica, earthquake.

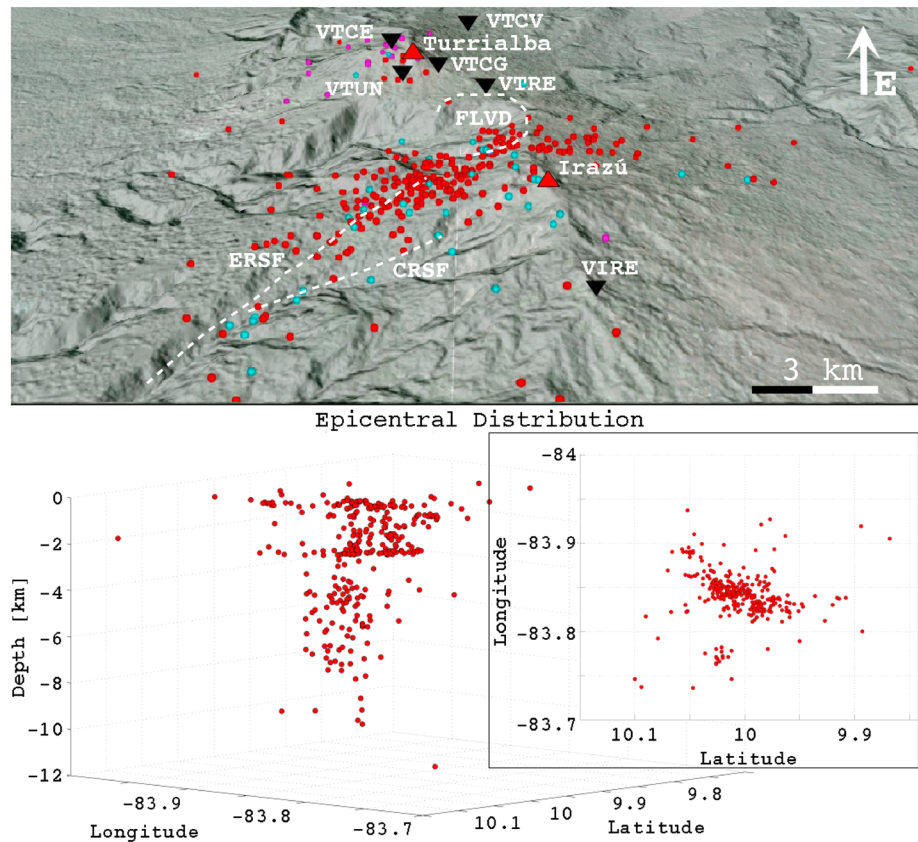


Figure 2. (top) Epicentral distribution of seismic events at the Irazú-Turrialba volcanic complex after the $M7.6$ Nicoya earthquake. Depth 0 refers to the sea level (i.e., ~ 3 km below the ground surface). Pink and red circles show the location of the seismic events before and after the $M7.6$ Nicoya earthquake, respectively. Turquoise circles represent the location of the seismic events the day after the Nicoya earthquake. Body wave arrivals were manually picked and located with SEISAN [Havskov and Ottemoller, 1999]. However, due to the limited number of stations, and their subaligned distribution, location accuracy is affected by up to ± 3 km errors laterally and vertically. The velocity model used is taken from Quintero and Kissling [2001].

2. Data

Before the $M7.6$ Nicoya earthquake, the seismic activity at the ITVC was mostly located beneath the NW flank of the Turrialba volcano with hybrid seismic events characterized by dominant frequencies between 4 Hz and 12 Hz, from 1 km to 8 km depth (pink events in Figure 2). After the main shock of the Nicoya earthquake a swarm sequence took place beneath the E flank of the Irazú volcano. Based on a spectrogram analysis the first local event occurred 40 s after the arrival of the P waves, which corresponds to the arrival of the S waves. We could not constrain this first motion further as it overlaps with the signal generated by the Nicoya main shock. The second local event ($M3.8$), the largest of the seismic sequence, occurred after the coda of the surface waves at 14:48 UTC. However, the swarm sequence only accelerated significantly after 14:57 UTC with 75 (locatable) seismic events occurred during the first hour (Figure 3). Nonlocatable events increase the total number of event occurrences to more than 110 events per hour.

Three pairs of aftershocks followed the main slip of the Nicoya earthquake approximately 1 h, 8 h, and 14 h after the main slip, respectively (Figure 3). The first pair of aftershocks ($M4.4$ and $M4.5$) struck during the peak of seismicity triggered by the main slip. Hence, we could not decouple seismic activity promoted by the main slip from the one promoted by the first pair of aftershocks. However, the following aftershocks triggered swarm activity along the fault plane inducing two peaks of 30 events per hour and 20 events per hour, respectively (Figure 3). Local earthquakes continued throughout the day and returned to normal levels

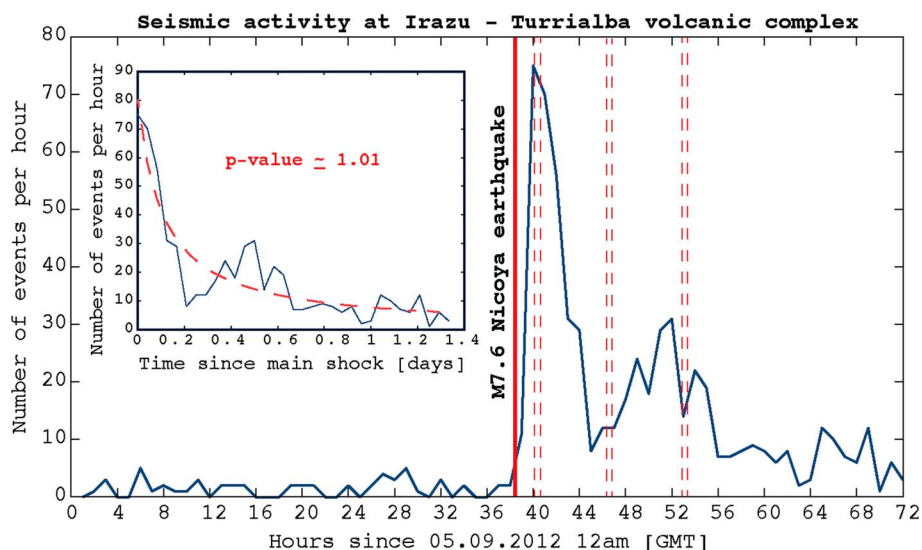


Figure 3. Cumulative number of seismic events triggered along the East Río Sucio Fault by the $M7.6$ Nicoya earthquake and its aftershocks (red dashed lines). The only $M \geq M4$ earthquake that shows a local earthquake within the waveform is the $M7.6$ earthquake (within the S waves). We could not recognize any local seismic event within any of the waveforms of the aftershocks. The increase of seismic activity that follows each pair of aftershocks is smooth, except for the first pair that is followed 11 min after by a sharp increase of local events. After the second and third pair of aftershocks the increase of local seismicity is less marked. Overall, the aftershock decay versus time fits an Omori's decay [Utsu, 1961], with k , c , and p of 8.5, 0.1, and 1.0173, respectively.

after approximately 30 h. A similar, but ambiguous, behavior was recorded in the same region on the 27 of August 2012 (04:37 UTC) after the $M7.3$ El Salvador earthquake. The dynamic stress

$$\sigma_D \sim \mu \cdot PGV \cdot v_s^{-1} \tag{1}$$

imposed by the $M7.3$ El Salvador earthquake was ~ 0.5 kPa (using v_s of 5300 m s^{-1}). Yet the local earthquake rate along the ERSF increased from an average of four events per hour to 12 events per hour after the earthquake. After the El Salvador earthquake the first seismic event at the ITVC occurred several hours (09:25 UTC) after the main shock. The number of local earthquakes grew to seven events per hour from 10:00 to 11:00 UTC reaching the peak of 13 events per hour from 10:00 UTC to 12:00 UTC. Then the seismic rate decreased back to seven, four, and two events per hour from 12:00 UTC to 13:00 UTC, 13:00 UTC to 14:00 UTC, and 14:00 UTC to 15:00 UTC, respectively.

The moment magnitude of the seismic events triggered by the Nicoya earthquake varies from $M0.5$ to $M3.5$, with a clear dominance of events between $M0.5$ and $M1.0$. Moment magnitude 0.5 is the magnitude threshold of detection for our array. Hypocentral depths vary from 10 km to 0 km (Figure 2), with the vast majority of the earthquakes being shallower than 5 km depth. The epicenters are distributed along a NW-NE region stretching from the southernmost part of the ERSF to the easternmost part of the Irazú volcanic edifice. This region showed a similar behavior after the $M7.3$ 1983, the $M7.0$ 1990, and the $M7.6$ 1991 earthquakes offshore Costa Rica.

3. Discussion

We performed a Coulomb stress analysis [Toda et al., 2011] to calculate the static stress imposed by the Nicoya earthquake on the ERSF. Due to the poor signal-to-noise ratio we could not invert for moment tensor solutions for the largest events of the seismic sequence presented here. Hence, we used as receiver fault subparallel to the arc the plane identified by the $M6.1$ earthquake that occurred on 8 January 2009 near the volcano Poás (strike, dip, and rake of 306, 86, and 150, respectively), with a friction coefficient of 0.6 and a depth of 10 km. The resulting Coulomb stress change imposed on the ITVC by the Nicoya earthquake is ~ 1 kPa. The variability associated with the specific values used for the shear modulus and for the velocity of the shear waves may induce small variations in the value of the dynamic stress associated with the passing S waves. However, the dynamic stress σ_D imposed at the ITVC by the passing S waves is 0.3 MPa (assuming

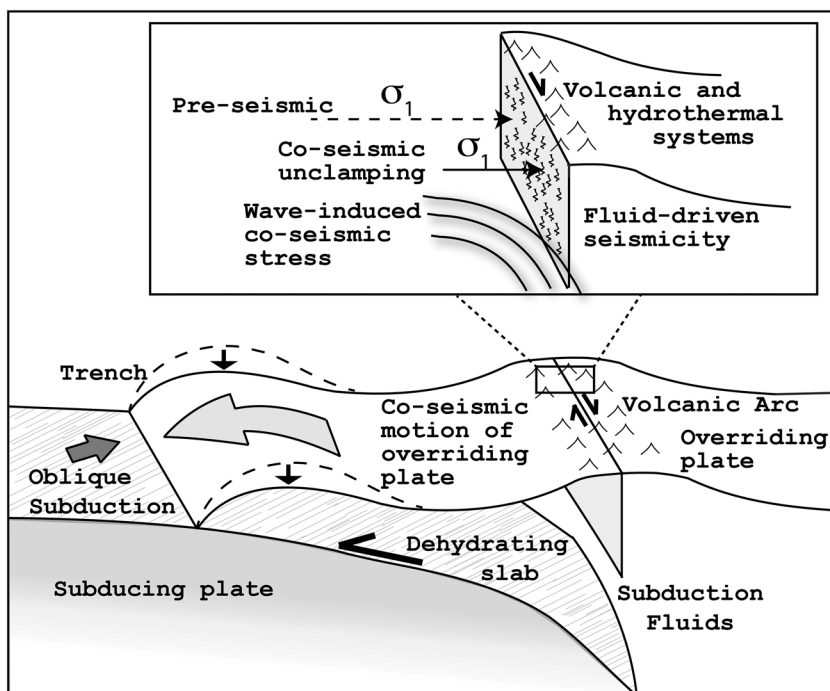


Figure 4. Coupled effects of elastic unloading and dynamic stress propagation. The reduction of the principal stress $\sigma_1 = \sigma_n$ from preseismic (dashed line) to coseismic (solid line) times translates into a reduction of the confining pressure on the fault plane. This promotes the reduction of the effective normal stress $\sigma_{n,eff}$ and facilitate the reactivation of the fault.

a shear modulus of 30 GPa, an average shear wave velocity of 5300 m s^{-1} according to *Quintero and Kissling* [2001] and a measured PGV of 0.05 m s^{-1} at the ITVC). This suggests that the seismicity triggered along the ERSF was not principally induced by static stress variations but rather by dynamic stress triggering.

The portion of the ERSF affected by the triggered seismic activity corresponds to the easternmost part of the Irazú volcanic edifice. In critically stressed volcanic environments, small variations of confining pressure may promote shear failure on optimally oriented fractures. Additionally, under such conditions the reduction of confining pressure may lead to an increase of the fluid pressure at depth (i.e., via gas phase exsolution) promoting hydrofracturing [*Sibson*, 1981] and vertical migration of hydrothermal fluids along the fault plane [*Lupi et al.*, 2011]. *Violay et al.* [2014] show that the presence of pore fluids strongly affects the initial frictional weakening promoting slip conditions at depth, particularly for small magnitude events (slip less than 0.5 m). Hence, variations as small as 0.3 MPa may have been sufficient to perturb this part of the ERSF that crosscuts the volcanic edifice of the Irazú volcano. Our findings are in agreement with recent conclusions of *Prejean* [2013] who points out that response of volcanic systems to incoming seismic energy is often observed on the sides of the volcanic edifice (i.e., in the hydrothermal systems or in groundwater reservoirs) rather than above the magmatic plumbing system.

Superimposed on the seismic dynamic trigger we also propose an effect due to the coseismic elastic deformation caused by the main slip. This mechanism would correspond to the “tectonic pull” described after megathrust earthquakes by recent authors. *Pritchard et al.* [2013] and *Takada and Fukushima* [2013] highlight that volcanic systems residing in volcanic arcs at convergent margins undergo a rapid subsidence (from days to months) immediately after the occurrence of a large magnitude subduction earthquake. This is also supported by continuous GPS measurements [*Vigny et al.*, 2011] that show uplift and subsidence of few centimeters at different regions in the volcanic arc during the Maule earthquake. A similar behavior was also observed by *Ikuta et al.* [2012] in Japan during the M9.0 Tohoku-Oki earthquake. *Lupi and Miller* [2014] suggest that at obliquely convergent margins lateral motion in the volcanic arc is promoted after part of the confining stress is removed by the megathrust slip. In oblique subduction zones, the shear stress is then accommodated in the overriding plate by trench-parallel, regional-scale, strike-slip faults that may be reactivated when the effective normal stress $\sigma_{n,eff}$ along the fault planes is reduced. However, contrary to the

Chilean and the Japanese cases, the Nicoya earthquake did not impose long-term Coulomb variations on the volcanic arc. Figure 4 suggests that over a short time window (i.e., less than a year), ignoring viscoelastic effects and assuming an elastic upper crust, the coseismic reduction of the normal stress σ_n imposed by the earthquake slip at the subduction interface may also affect distant faults facing the region of main slip of the earthquake. In this case fault unclamping may not be large magnitude (i.e., 1 kPa) but may still facilitate shear failure. In addition, upwelling fluids can ultimately reduce the effective normal stress $\sigma_{n,eff}$ along the fault plane further. This would support the observation of peaks of seismic activity following the major aftershocks of the Nicoya earthquake (Figure 3). The effects of $\sim M4.5$ earthquakes have been suggested to be negligible for distances larger than 30 km from the epicenter [Manga et al., 2009]. Yet, Figure 3 shows two clear peaks of increased seismic activity after the major aftershocks of the Nicoya earthquake. Recent laboratory experiments at elevated slip rates show that friction may reduce as low as 0.05 once the fault plane is reactivated [Di Toro et al., 2011]. Hence, in fault systems where friction is reduced, less seismic energy may be required to trigger seismic activity remotely.

4. Conclusion

Examining the seismic records from the OVSICORI seismic network around the Irazú-Turrialba volcanic complex before, during, and after the $M7.6$ Nicoya earthquake we find evidence of triggered seismic activity. The seismicity is remarkably higher (more than 300 locatable earthquakes within 24 h) if compared to the normal seismic rate of five to six events per day normally occurring at the ITVC. The seismic rate triggered by the Nicoya megathrust earthquake is also larger than the peaks of seismicity sometimes observed at the ITVC that reach a maximum of 150 of events during the entire seismic series that may last from 1 to 5 days. The epicenters of the events triggered by the Nicoya earthquake are distributed along the southernmost part of the East Rio Sucio Fault system, a right-lateral strike-slip fault that joins the Finca Liebres Volcanic Depression between the Irazú and Turrialba volcanic edifices. The calculated static stress imposed by the $M7.6$ Nicoya earthquake on a fault plane subparallel to the southernmost end of the East Rio Sucio Fault was smaller than the dynamic stress imposed by the passing seismic waves. The maximum dynamic stress was in the order of 0.3 MPa and may have been the principal factor that determined the reactivation of the fault. However, we suggest that under the assumption of an elastic upper crust, the coseismic reduction of the normal stress σ_n imposed by the main slip at the subduction interface may also have affected this part of the fault system. Due to the swarm-like character of the seismic sequence and the likely presence of a fluid circulation system maintained by the elevated geothermal gradient of the area, we suggest that the triggered seismic activity may have involved fluid mobilization.

The decay of the number of seismic events along the East Rio Sucio Fault follows an Omori's decay. However, we point out that powerful aftershocks of the Nicoya earthquake (i.e., $\sim M4.5$) also affected and enhanced seismic activity along the fault as suggested by peaks of seismic activity up to 14 h after the main shock. This may be favored by the coupled effects of a reduced friction of the reactivated East Rio Sucio Fault and the result of shear failure due to increased fluid pressure.

Acknowledgments

Nima Riahi is thanked for technical support and discussion. Matteo Lupi thanks the ETH Zurich Postdoctoral Fellowship Program for financial support. The raw data are hosted on a server of the ETH of Zurich and can be accessed by downloading the freeware software at <http://www.bittorrent.com/sync/downloads> and using the access code BU72QBCEU2DEML5DXGCSHCKK54A QOOTR2. The authors thank David Hill, Thomas Walter, and an anonymous reviewer for the constructive comments.

The Editor thanks David Hill, Thomas Walter, and an anonymous reviewer for their assistance in evaluating this paper.

References

- Alvarado, G. E., M. J. Carr, B. D. Turrin, C. C. Swisher, H. Schmincke, and K. W. Hudnut (2006), Recent volcanic history of Irazú volcano, Costa Rica: Alternation and mixing of two magma batches, and pervasive mixing, *GSA Special Papers*, 412, 259–276.
- Corti, G., E. Carminati, F. Mazzarini, and M. O. Garcia (2005), Active strike-slip faulting in El Salvador, Central America, *Geology*, 33(12), 989–992.
- Delle Donne, D., A. J. Harris, M. Ripepe, and R. Wright (2010), Earthquake-induced thermal anomalies at active volcanoes, *Geology*, 38(9), 771–774.
- Di Toro, G., R. Han, T. Hirose, N. De Paola, S. Nielsen, K. Mizoguchi, F. Ferri, M. Cocco, and T. Shimamoto (2011), Fault lubrication during earthquakes, *Nature*, 471(7339), 494–498.
- Dziak, R. P., W. W. Chadwick, C. G. Fox, and R. W. Embley (2003), Hydrothermal temperature changes at the Southern Juan de Fuca ridge associated with Mw 6.2 Blanco transform earthquake, *Geology*, 31(2), 119–122.
- Eggert, S., and T. Walter (2009), Volcanic activity before and after large tectonic earthquakes: Observations and statistical significance, *Tectonophysics*, 471(1–2), 14–26.
- Havskov, J., and L. Ottemoller (1999), Seisan earthquake analysis software, *Seismol. Res. Lett.*, 70(5), 532–534.
- Hill, D., and S. Prejean (2007), Dynamic triggering, in *Treatise on Geophysics*, vol. 4 Earthquake Seismology, edited by H. Kanamori and G. Schubert, pp. 257–291, Elsevier, Amsterdam, Netherlands.
- Hill, D., F. Pollitz, and C. Newhall (2002), Earthquake-volcano interactions, *Phys. Today*, 55(11), 41–47.
- Husen, S., S. Wiemer, and R. B. Smith (2004), Remotely triggered seismicity in the Yellowstone National Park Region by the 2002 Mw 7.9 Denali fault earthquake, Alaska, *Bull. Seismol. Soc. Am.*, 94(6B), S317–S331.
- Ikuta, R., M. Satomura, A. Fujita, S. Shimada, and M. Ando (2012), A small persistent locked area associated with the 2011 Mw 9.0 Tohoku-Oki earthquake, deduced from GPS data, *J. Geophys. Res.*, 117, B11408, doi:10.1029/2012JB009335.

- Johnson, H. P., M. Hutnak, R. P. Dziak, C. G. Fox, I. Urcuyo, J. P. Cowen, J. Nabelek, and C. Fisher (2000), Earthquake-induced changes in a hydrothermal system on the Juan de Fuca mid-ocean ridge, *Nature*, *407*(6801), 174–177.
- Lewis, J. C., A. C. Boozer, A. López, and W. Montero (2008), Collision versus sliver transport in the hanging wall at the Middle America subduction zone: Constraints from background seismicity in central Costa Rica, *Geochem. Geophys. Geosyst.*, *9*(7), Q07S06, doi:10.1029/2007GC001711.
- Linde, A. T., and I. S. Sacks (1998), Triggering of volcanic eruptions, *Nature*, *395*(6705), 888–890.
- Lupi, M., and S. A. Miller (2014), Short-lived tectonic switch mechanism for long-term pulses of volcanic activity after mega-thrust earthquakes, *Solid Earth*, *5*, 13–24.
- Lupi, M., S. Geiger, and C. Graham (2011), Numerical simulations of seismicity-induced fluid flow in the Tjörnes Fracture Zone, Iceland, *J. Geophys. Res.*, *116*, B07101, doi:10.1029/2010JB007732.
- Lupi, M., E. Saenger, F. Fuchs, and S. Miller (2013), Lusi mud eruption triggered by geometric focusing of seismic waves, *Nat. Geosci.*, *6*(8), 642–646.
- Manga, M., and M. Bonini (2012), Large historical eruptions at subaerial mud volcanoes, Italy, *Nat. Hazards Earth Syst. Sci.*, *12*, 3377–3386.
- Manga, M., and E. Brodsky (2006), Seismic triggering of eruptions in the far field: Volcanoes and geysers, *Annu. Rev. Earth Planet. Sci.*, *34*, 263–291.
- Manga, M., M. Brumm, and M. Rudolph (2009), Earthquake triggering of mud volcanoes, *Mar. Pet. Geol.*, *26*(9), 1785–1798.
- Marzocchi, W., E. Casarotti, and A. Piersanti (2002), Modeling the stress variations induced by great earthquakes on the largest volcanic eruptions of the 20th century, *J. Geophys. Res.*, *2320*(B11), doi:10.1029/2001JB001391.
- Matsumoto, N., G. Kitagawa, and E. Roeloffs (2003), Hydrological response to earthquakes in the Haibara well, central Japan—I. Ground-water level changes revealed using state space decomposition of atmospheric pressure, rainfall and tidal responses, *Geophys. J. Int.*, *155*(3), 885–898.
- Mazzini, A., H. Svensen, G. G. Akhmanov, G. Aloisi, S. Planke, A. Malthe-Sørensen, and B. Istadi (2007), Triggering and dynamic evolution of the LUSI mud volcano, Indonesia, *Earth Planet. Sci. Lett.*, *261*(3–4), 375–388.
- Montero, P. W., J. C. Lewis, J. S. Marshall, S. Kruse, and P. Wetmore (2013), Neotectonic faulting and forearc sliver motion along the Atirro-Rio Sucio fault system, Costa Rica, Central America, *Geol. Soc. Am. Bull.*, *125*(5–6), 857–876.
- Prejean, S. G. (2013), Where do we stand after twenty years of dynamic triggering studies, Abstract S43D-04 paper presented at 2013 Fall Meeting, AGU, San Francisco, Calif.
- Pritchard, M., J. Jay, F. Aron, S. Henderson, and L. Lara (2013), Subsidence at southern Andes volcanoes induced by the 2010 Maule, Chile earthquake, *Nat. Geosci.*, *6*(8), 632–636.
- Protti, M., V. González, A. V. Newman, T. H. Dixon, S. Y. Schwartz, J. S. Marshall, L. Feng, J. I. Walter, R. Malservisi, and S. E. Owen (2014), Nicoya earthquake rupture anticipated by geodetic measurement of the locked plate interface, *Nat. Geosci.*, *7*(2), 117–121.
- Quintero, R., and E. Kissling (2001), An improved P-wave velocity reference model for Costa Rica, *Geophys. Res. Lett.*, *28*(1), 3–20.
- Roeloffs, E. A. (1998), Persistent water level changes in a well near Parkfield, California, due to local and distant earthquakes, *J. Geophys. Res.*, *103*(B1), 869–889.
- Sibson, R. H. (1981), Controls on low-stress hydro-fracture dilatancy in thrust, wrench and normal fault terrains, *Nature*, *289*, 665–667.
- Takada, Y., and Y. Fukushima (2013), Volcanic subsidence triggered by the 2011 Tohoku earthquake in Japan, *Nat. Geosci.*, *6*(8), 637–641.
- Toda, S., R. S. Stein, V. Sevilgen, and J. Lin (2011), Coulomb 3. 3 graphic-rich deformation and stress-change software for earthquake, tectonic, and volcano research and teaching—User guide. *U.S. Geol. Surv. Open-File Rep. 2011–1060*, U.S. Geol. Surv., Menlo Park, Calif.
- Utsu, T. (1961), A statistical study on the occurrence of aftershocks, *Geophys. Mag.*, *30*, 521–605.
- van der Elst, N. J., H. M. Savage, K. M. Keranen, and G. A. Abers (2013), Enhanced remote earthquake triggering at fluid-injection sites in the Midwestern United States, *Science*, *341*(6142), 164–167.
- Vigny, C., et al. (2011), The 2010 *M*_w 8.8 Maule megathrust earthquake of Central Chile, monitored by GPS, *Science*, *332*(6036), 1417–1421.
- Violay, M., S. Nielsen, B. Gibert, E. Spagnuolo, A. Cavallo, P. Azais, S. Vinciguerra, and G. Di Toro (2014), Effect of water on the frictional behavior of cohesive rocks during earthquakes, *Geology*, *42*(1), 27–30.
- Walter, T., R. Wang, M. Zimmer, H. Grosse, B. Lühr, and A. Ratdomopurbo (2007), Volcanic activity influenced by tectonic earthquakes: Static and dynamic stress triggering at Mt. Merapi, *Geophys. Res. Lett.*, *34*(5), L05304, doi:10.1029/2006GL028710.
- Wang, C. (2007), Liquefaction beyond the near field, *Seismol. Res. Lett.*, *78*(5), 512–517.
- Wang, C.-Y., and M. Manga (2010), Hydrologic responses to earthquakes and a general metric, *Geofluids*, *10*(1–2), 206–216.
- Weatherley, D. K., and R. W. Henley (2013), Flash vaporization during earthquakes evidenced by gold deposits, *Nat. Geosci.*, *6*(4), 294–298.
- Weingarten, M., and S. Ge (2014), Insights into water level response to seismic waves: A 24 year high-fidelity record of global seismicity at devils hole, *Geophys. Res. Lett.*, *41*, 74–80, doi:10.1002/2013GL058418.
- West, M., J. J. Sánchez, and S. R. McNutt (2005), Periodically triggered seismicity at Mount Wrangell, Alaska, after the Sumatra earthquake, *Science*, *308*(5725), 1144–1146.
- Yue, H., T. Lay, S. Y. Schwartz, L. Rivera, M. Protti, T. H. Dixon, S. Owen, and A. V. Newman (2013), The 5 September 2012 Nicoya, Costa Rica *M*_w 7.6 earthquake rupture process from joint inversion of high-rate GPS, strong-motion, and teleseismic *P* wave data and its relationship to adjacent plate boundary interface properties, *J. Geophys. Res. Solid Earth*, *118*, 5453–5466, doi:10.1002/jgrb.50379.